RESEARCH ARTICLE

Influence of Magnetic Field in Three-Dimensional Flow of Couple Stress Nanofluid over a Nonlinearly Stretching Surface with Convective Condition

Tasawar Hayat[1,2], Arsalan Aziz[1], Taseer Muhammad[1]*, Bashir Ahmad[2]

1 Department of Mathematics, Quaid-I-Azam University 45320, Islamabad, Pakistan, 2 Nonlinear Analysis and Applied Mathematics (NAAM) Research Group, Faculty of Science, King Abdulaziz University, Jeddah, Saudi Arabia

* taseer_qau@yahoo.com

Abstract

This article investigates the magnetohydrodynamic (MHD) three-dimensional flow of couple stress nanofluid subject to the convective boundary condition. Flow is generated due to a nonlinear stretching of the surface in two lateral directions. Temperature and nanoparticles concentration distributions are studied through the Brownian motion and thermophoresis effects. Couple stress fluid is considered electrically conducting through a non-uniform applied magnetic field. Mathematical formulation is developed via boundary layer approach. Nonlinear ordinary differential systems are constructed by employing suitable transformations. The resulting systems have been solved for the convergent series solutions of velocities, temperature and nanoparticles concentration profiles. Graphs are sketched to see the effects of different interesting flow parameters on the temperature and nanoparticles concentration distributions. Numerical values are computed to analyze the values of skin-friction coefficients and Nusselt number.

Introduction

Boundary layer flow over a continuous stretching surface has various industrial and engineering applications. Such flow commonly involves in the paper production, wire drawing, glass fiber production, extrusion of plastic sheets, hot rolling, cooling of a metallic plate in a cooling bath and many others. Many researchers have discussed the different problems through the linear stretching of the surface but there are various situations in the industrial and technological processes where the stretching of the surface is not necessarily linear. Particularly the flow induced by a nonlinear stretching surface has played important role in the polymer extrusion process. With this viewpoint Vajravelu [1] provided a study to examine the flow and heat transfer properties of viscous fluid induced by a nonlinear stretching surface. Cortell [2] performed a numerical study to investigate the flow of viscous fluid over a nonlinear stretching

surface. He studied the two cases of heat transfer namely the constant surface temperature and the prescribed surface temperature. Cortell [3] also explored the flow of viscous fluid over a nonlinearly stretching surface in the presence of viscous dissipation and radiation effects. Hayat et al. [4] addressed the magnetohydrodynamic (MHD) flow over a nonlinear stretching surface by using the modified Adomian decomposition and Padé approximation techniques. Flow and heat transfer properties of nanofluid over a nonlinear stretching surface is reported by Rana and Bhargava [5]. Mukhopadhyay [6] discussed the boundary layer flow over a permeable nonlinear stretching surface subject to partial slip condition. Mabood et al. [7] studied the MHD flow of water-based nanofluid over a nonlinear stretching surface in the presence of viscous dissipation. Recently Mustafa et al. [8] investigated the flow of nanofluid over a nonlinearly stretching surface subject to the convective surface boundary condition.

The insertion of ultrafine nanoparticles (<100nm) in the base liquid is termed as nanofluid. The nanoparticles utilized in nanofluids are basically made of metals (Cu, Al, Ag), oxides (Al_2O_3) carbides (SiC), nitrides (SiN, AlN) or nonmetals (carbon nanotubes, graphite) and the base liquids like water, oil or ethylene glycol. Addition of nanoparticles in the base liquids greatly enhances the thermal characteristics of the base liquids. Due to such interesting properties, nanofluids are useful in various industrial and technological processes such as the cooling of electronic devices, transformer cooling, vehicle cooling, heat exchanger, nuclear reactor, biomedicine and many others. Especially the magneto nanofluids are useful in MHD power generators, removal of blockage in the arteries, hyperthermia, cancer tumor treatment, magnetic resonance imaging etc. The term nanofluid was first introduced by Choi and Eastman [9] and they illustrated that the thermal properties of base liquids are enhanced when we add up the nanoparticles in it. Boungiorno [10] constructed a mathematical expression to investigate the thermal characteristics of base fluids. Here the effects of thermophoresis and Brownian motion are utilized to enhance the thermal properties of base liquids. Khan and Pop [11] employed the Boungiorno model [10] to analyze the boundary layer flow of nanofluid over a stretching surface. Pujari et al. [12] studied the orientation state of multiwalled carbon nanotubes (MWNTs) dispersions in steady and transient shear flows. Dong and Cao [13] examined the anomalous orientations of rigid carbon nanotube in a sheared fluid. Zhao et al. [14] reported both theoretical and experimental studies of collective effects on the Soret coefficient of particles in deionized (DI) water. Translational thermophoresis and rotational movement of peanut-like colloids under the influence of temperature gradient is addressed by Dong et al. [15]. Wang et al. [16] discussed the thermal diffusion behavior of dilute solutions of very long and thin charged colloidal rods by using the holographic grating technique. Few more recent studies in this direction can be quoted through the investigations [17–27] and several refs. therein.

Most of the studies in the literature explain viscous materials by the classical Navier-Stokes relations. There are several complex rheological materials such as paints, shampoos, slurries, toothpastes, polymer solutions, ketchup, paper pulp, blood, greases, drilling muds, lubricating oils and many others that cannot be characterized through the classical Navier-Stokes expressions. Such materials are known as the non-Newtonian fluids. However, there is no single relation that can present the characteristics of all non-Newtonian fluids. Hence various models of non-Newtonian fluids are developed in the literature. The couple stress fluid model [28–33] is one of such materials. This model has important features due to the presence of body couples, couple stresses and non-symmetric stress tensor. Some interesting examples of the couple stress fluid are blood, suspension fluids, lubricants and electro rheological fluids.

The main aim of the present communication is to generalize the analysis of ref. [8] into three directions. Firstly to consider the three-dimensional flow of couple stress nanofluid. Effects of Brownian motion and thermophoresis are present. We imposed the thermal convective [34,35] and zero nanoparticles mass flux conditions at the surface [36,37]. Secondly to

analyze the influence of variable magnetic field under low magnetic Reynolds number assumption. Thirdly to compute the convergent series solutions through the homotopy analysis technique (HAM) [38–45]. Effects of various emerging parameters on the temperature and nanoparticles concentration distributions are sketched and discussed. Skin-friction coefficients and Nusselt number are computed numerically.

Problem Formulation

Let us consider the steady three-dimensional flow of an incompressible couple stress nanofluid by a bidirectional nonlinear stretching surface. The couple stress fluid is assumed an electrically conducting through a non-uniform magnetic field applied in the $z-$direction. Effects of electric field and Hall current are neglected. The induced magnetic field is not considered subject to the small magnetic Reynolds number. Brownian motion and thermophoresis effects are present. Consider the Cartesian coordinate system in such a way that the $x-$ and $y-$axes are taken along the stretched sheet and $z-$axis is perpendicular to it. Let $U_w(x,y) = a(x+y)^n$ and $V_w(x,y) = b(x+y)^n$ denote the surface stretching velocities along the $x-$ and $y-$directions respectively with $a, b, n > 0$ as the constants. The temperature at the surface is controlled through a convective heating mechanism which is denoted via heat transfer coefficient h_f and temperature of the hot fluid T_f below the surface. The boundary layer expressions governing the flow of couple stress nanofluid are given by

$$\frac{\partial u}{\partial x} + \frac{\partial v}{\partial y} + \frac{\partial w}{\partial z} = 0, \tag{1}$$

$$u\frac{\partial u}{\partial x} + v\frac{\partial u}{\partial y} + w\frac{\partial u}{\partial z} = \nu\frac{\partial^2 u}{\partial z^2} - \nu\prime\frac{\partial^4 u}{\partial z^4} - \frac{\sigma B^2(x,y)}{\rho_f}u, \tag{2}$$

$$u\frac{\partial v}{\partial x} + v\frac{\partial v}{\partial y} + w\frac{\partial v}{\partial z} = \nu\frac{\partial^2 v}{\partial z^2} - \nu\prime\frac{\partial^4 v}{\partial z^4} - \frac{\sigma B^2(x,y)}{\rho_f}v, \tag{3}$$

$$u\frac{\partial T}{\partial x} + v\frac{\partial T}{\partial y} + w\frac{\partial T}{\partial z} = \alpha\frac{\partial^2 T}{\partial z^2} + \frac{(\rho c)_p}{(\rho c)_f}\left(D_B\left(\frac{\partial T}{\partial z}\frac{\partial C}{\partial z}\right) + \frac{D_T}{T_\infty}\left(\frac{\partial T}{\partial z}\right)^2\right), \tag{4}$$

$$u\frac{\partial C}{\partial x} + v\frac{\partial C}{\partial y} + w\frac{\partial C}{\partial z} = D_B\left(\frac{\partial^2 C}{\partial z^2}\right) + \frac{D_T}{T_\infty}\left(\frac{\partial^2 T}{\partial z^2}\right). \tag{5}$$

The subjected boundary conditions are

$$u = U_w(x,y), \quad v = V_w(x,y), \quad w = 0, \quad -k\frac{\partial T}{\partial z} = h_f(T_f - T), \quad D_B\frac{\partial C}{\partial z} + \frac{D_T}{T_\infty}\frac{\partial T}{\partial z} = 0 \text{ at } z = 0, \tag{6}$$

$$u \to 0, \quad v \to 0, \quad T \to T_\infty, \quad C \to C_\infty \text{ as } z \to \infty. \tag{7}$$

Note that u, v and w are the velocity components in the $x-$, $y-$ and $z-$directions respectively, $\nu\ (= \mu/\rho_f)$ represents the kinematic viscosity, μ stands for dynamic viscosity, ρ_f represents the density of base fluid, $\nu\prime\ (= n^*/\rho_f)$ denotes the couple stress viscosity, n^* stands for couple stress viscosity parameter, σ denotes the electrical conductivity, $B(x,y) = B_0(x+y)^{\frac{n-1}{2}}$ stands for non-uniform magnetic field, T denotes the temperature, $\alpha = k/(\rho c)_f$ represents the thermal diffusivity of fluid, k stands for thermal conductivity of fluid, $(\rho c)_f$ represents the heat capacity of

fluid, $(\rho c)_P$ denotes the effective heat capacity of nanoparticles, D_B stands for Brownian diffusion coefficient, C denotes the nanoparticles concentration, D_T represents the thermophoretic diffusion coefficient, $h_f = h(x + y)^{\frac{n-1}{2}}$ denotes the non-uniform heat transfer coefficient, T_∞ represents the temperature far away from the surface and C_∞ represents the nanoparticles concentration far away from the surface. We now use the following transformations

$$u = a(x + y)^n f'(\eta), \quad v = a(x + y)^n g'(\eta),$$

$$w = -\left(\frac{av(n+1)}{2}\right)^{\frac{1}{2}}(x+y)^{\frac{n-1}{2}}\left\{(f+g) + \frac{n-1}{n+1}\eta(f'+g')\right\}, \tag{8}$$

$$\theta(\eta) = \frac{T - T_\infty}{T_f - T_\infty}, \quad \phi(\eta) = \frac{C - C_\infty}{C_\infty}, \quad \eta = \left(\frac{a(n+1)}{2v}\right)^{\frac{1}{2}}(x+y)^{\frac{n-1}{2}} z.$$

Eq (1) is now satisfied and Eqs (2)–(7) have the following forms

$$f''' + (f + g)f'' - \frac{2n}{n+1}(f' + g')f' - Kf^{(v)} - M^2 f' = 0, \tag{9}$$

$$g''' + (f + g)g'' - \frac{2n}{n+1}(f' + g')g' - Kg^{(v)} - M^2 g' = 0, \tag{10}$$

$$\theta'' + Pr((f + g)\theta' + Nb\theta'\phi' + Nt\theta'^2) = 0, \tag{11}$$

$$\phi'' + LePr(f + g)\phi' + \frac{Nt}{Nb}\theta'' = 0, \tag{12}$$

$$f(0) = g(0) = 0, \ f'(0) = 1, \ g'(0) = c, \ \theta'(0) = -\gamma(1 - \theta(0)), \ Nb\phi'(0) + Nt\theta'(0) = 0, \tag{13}$$

$$f'(\infty) \to 0, \ g'(\infty) \to 0, \ \theta(\infty) \to 0, \ \phi(\infty) \to 0. \tag{14}$$

In above expressions K denotes the couple stress parameter, M represents the magnetic number, c stands for ratio parameter, Pr denotes the Prandtl number, Nb represents the Brownian motion parameter, Nt stands for thermophoresis parameter, γ denotes the Biot number, Le stands for Lewis number and prime denotes the differentiation with respect to η. These variables are defined by

$$K = \frac{(n+1)v'a}{2v^2}(x+y)^{n-1}, \quad M^2 = \frac{2\sigma B_0^2}{a\rho_f(n+1)}, \quad c = \frac{b}{a}, \quad Pr = \frac{v}{\alpha},$$

$$Nb = \frac{(\rho c)_p D_B C_\infty}{(\rho c)_f v}, \quad Nt = \frac{(\rho c)_p D_T(T_f - T_\infty)}{(\rho c)_f v T_\infty}, \quad \gamma = \frac{h_f}{k}\sqrt{\frac{v}{a}}, \quad Le = \frac{\alpha}{D_B}. \tag{15}$$

Skin-friction coefficients and local Nusselt number are given by

$$Re_x^{1/2}C_{fx} = \left(\frac{n+1}{2}\right)^{1/2}(f''(0) - Kf^{iv}(0)),$$

$$Re_y^{1/2}C_{fy} = c^{-3/2}\left(\frac{n+1}{2}\right)^{1/2}(g''(0) - Kg^{iv}(0)),$$

$$Re_x^{-1/2}Nu_x = -\left(\frac{n+1}{2}\right)^{1/2}\theta'(0).$$

(16)

It is seen that the dimensionless mass flux denoted by a Sherwood number Sh_x is now identically zero and $Re_x = U_w(x+y)/v$ and $Re_y = V_w(x+y)/v$ represent the local Reynolds numbers.

Series Solutions

Our purpose now is to compute the series solutions via homotopy analysis technique (HAM). The appropriate initial guesses $(f_0, g_0, \theta_0, \phi_0)$ and the corresponding auxiliary linear operators $(\mathbf{L}_f, \mathbf{L}_g, \mathbf{L}_\theta, \mathbf{L}_\phi)$ for homotopic solutions are selected as follows:

$$f_0(\eta) = 1 - e^{-\eta}, \ \ g_0(\eta) = c(1 - e^{-\eta}), \ \ \theta_0(\eta) = \frac{\gamma}{1+\gamma}e^{-\eta}, \ \ \phi_0(\eta) = -\frac{\gamma}{1+\gamma}\frac{Nt}{Nb}e^{-\eta}, \quad (17)$$

$$\mathbf{L}_f = f''' - f', \mathbf{L}_g = g''' - g', \ \ \mathbf{L}_\theta = \theta'' - \theta, \mathbf{L}_\phi = \phi'' - \phi. \quad (18)$$

The above operators have the following properties

$$\mathbf{L}_f[B_1 + B_2 e^\eta + B_3 e^{-\eta}] = 0, \mathbf{L}_g[B_4 + B_5 e^\eta + B_6 e^{-\eta}] = 0,$$
$$\mathbf{L}_\theta[B_7 e^\eta + B_8 e^{-\eta}] = 0, \ \ \mathbf{L}_\phi[B_9 e^\eta + B_{10} e^{-\eta}] = 0.$$

(19)

in which B_i ($i = 1 - 10$) depict the arbitrary constants.

Convergence Analysis

No doubt the auxiliary parameters in the series solutions have key role regarding convergence. The proper values of these parameters play a key role to develop the convergent series solutions. For such interest, the $\hbar$- curves for the velocities, temperature and nanoparticles concentration profiles are plotted at 15th order of deformations. Figs 1 and 2 clearly indicate that the interval of convergence for f, g, θ and ϕ are [-1.50, -0.15], [-1.50, -0.20], [-1.75, -0.15] and [-1.80, -0.20] respectively. Table 1 presents that the 10th order of deformations is enough for the series solutions of velocities, temperature and nanoparticles concentration profiles.

Results and Discussion

Effects of couple stress parameter K, magnetic number M, ratio parameter c, Biot number γ, Lewis number Le, Prandtl number Pr, Brownian motion parameter Nb and thermophoresis parameter Nt on the dimensionless temperature $\theta(\eta)$ and nanoparticles concentration $\phi(\eta)$ are sketched in the Figs 3–16. The results are obtained for two different values of n just to compare the corresponding profiles in cases of linear and nonlinear stretching surfaces. Fig 3 presents the temperature profiles corresponding to different values of couple stress parameter K. Temperature profiles are enhanced for the larger values of couple stress parameter. Moreover the temperature profile is weaker at $n = 1.0$ than at $n = 1.5$. Fig 4 depicts the temperature profiles for various values of magnetic number M. Here $M \neq 0$ corresponds to the hydromagnetic flow case and $M = 0$ is for the hydrodynamic flow situation. We examined that the temperature
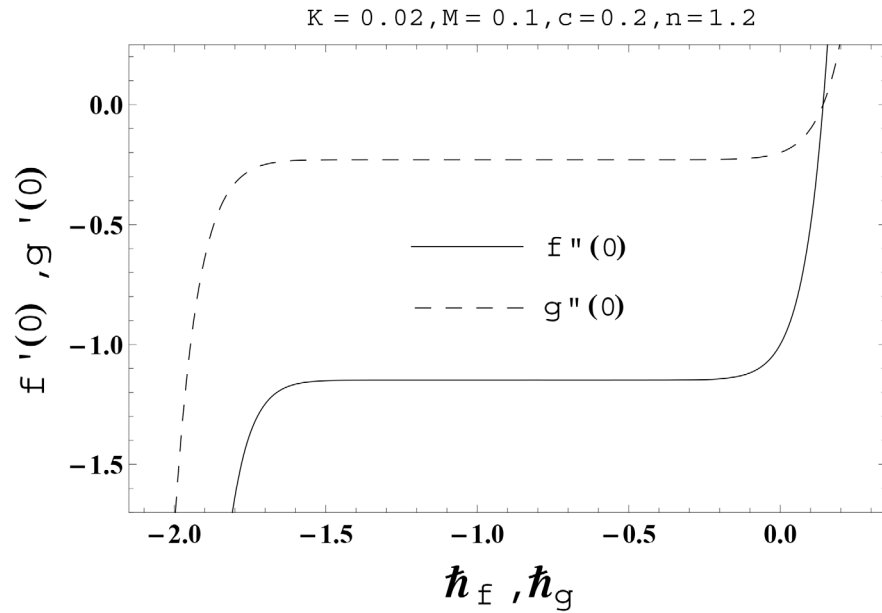
Fig 1. The $\hbar$-curves for the functions $f(\eta)$ and $g(\eta)$.

profiles are higher for hydromagnetic flow in comparison to the hydrodynamic flow. An increase in the values of magnetic number causes stronger temperature profiles. Moreover the thermal boundary layer thickness is lower in linear stretching surface case ($n = 1.0$) when compared with the nonlinear stretching surface case ($n = 1.5$). Fig 5 shows the temperature profiles
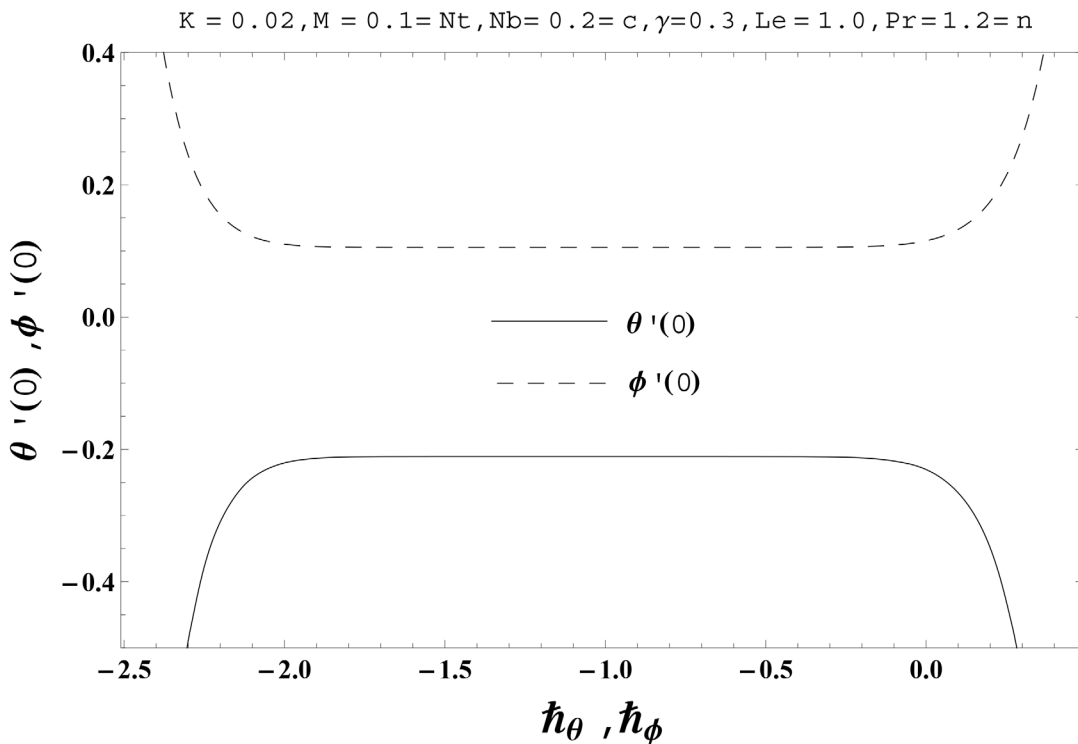

Fig 2. The $\hbar$-curves for the functions $\theta(\eta)$ and $\phi(\eta)$.

Table 1. Convergence of series solutions for various order of approximations when $K = 0.02$, $M = 0.1 = Nt$, $c = 0.2 = Nb$, $\gamma = 0.3$, $Le = 1.0$ and $Pr = 1.2 = n$.

Order of approximations	$-f''(0)$	$-g''(0)$	$-\theta'(0)$	$\phi'(0)$
1	1.15136	0.23027	0.21692	0.10846
5	1.14888	0.22978	0.21084	0.10542
10	1.14887	0.22977	0.21078	0.10539
20	1.14887	0.22977	0.21078	0.10539
35	1.14887	0.22977	0.21078	0.10539
50	1.14887	0.22977	0.21078	0.10539

doi:10.1371/journal.pone.0145332.t001

for different values of ratio parameter *c*. Larger values of ratio parameter creates a reduction in the temperature profiles and related thermal boundary layer thicknesses. For *c* = 0, the two-dimensional flow situation is achieved. It is also noticed that the temperature profiles for two-dimensional flow are lower when compared with the three-dimensional situation. Fig 6 presents the temperature profiles for various values of the Biot number *γ*. Here the temperature profiles are enhanced when we increase the values of Biot number. An increase in the Biot number *γ* causes stronger convection which shows higher temperature profiles and more thermal boundary layer thicknesses. It is also seen that the temperature profiles show similar behavior for both linear and nonlinear stretching surfaces. Fig 7 depicts that the temperature profiles are lower for the larger values of Prandtl number *Pr*. Prandtl number has an inverse relationship with the thermal diffusivity. An enhancement in the Prandtl number causes a weaker thermal diffusivity. Such weaker thermal diffusivity corresponds to lower temperature profiles and thermal boundary layer thicknesses. Moreover the thermal boundary layer thickness is less for linear stretching surface (*n* = 1.0) in comparison to the nonlinear stretching surface (*n* = 1.5). Fig 8 shows the temperature profiles for different values of thermophoresis parameter *Nt*. Temperature profiles are enhanced when we increase the values of
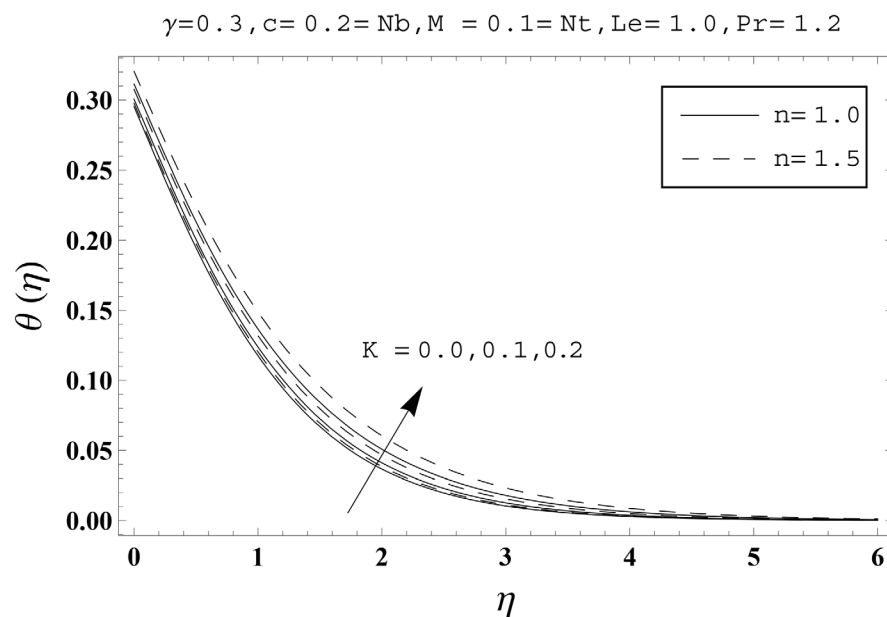

Fig 3. Effects of *n* and *K* on *θ*(*η*).

doi:10.1371/journal.pone.0145332.g003

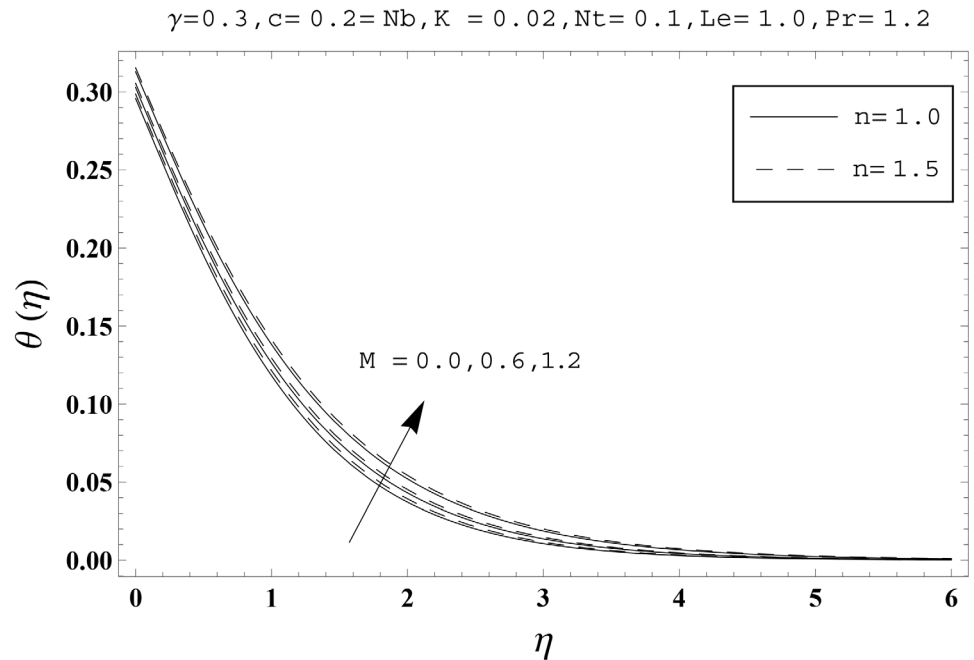$\gamma = 0.3, c = 0.2 = Nb, K = 0.02, Nt = 0.1, Le = 1.0, Pr = 1.2$

Fig 4. Effects of *n* and *M* on *θ(η)*.

doi:10.1371/journal.pone.0145332.g004

thermophoresis parameter. Larger values of *Nt* causes a stronger thermophoresis force which tends to move nanoparticles from hot to cold region and as a result the temperature profile enhances. It is also observed that the thermal boundary layer thicknesses show similar behavior for both linear and nonlinear stretching surfaces. Fig 9 presents the nanoparticles
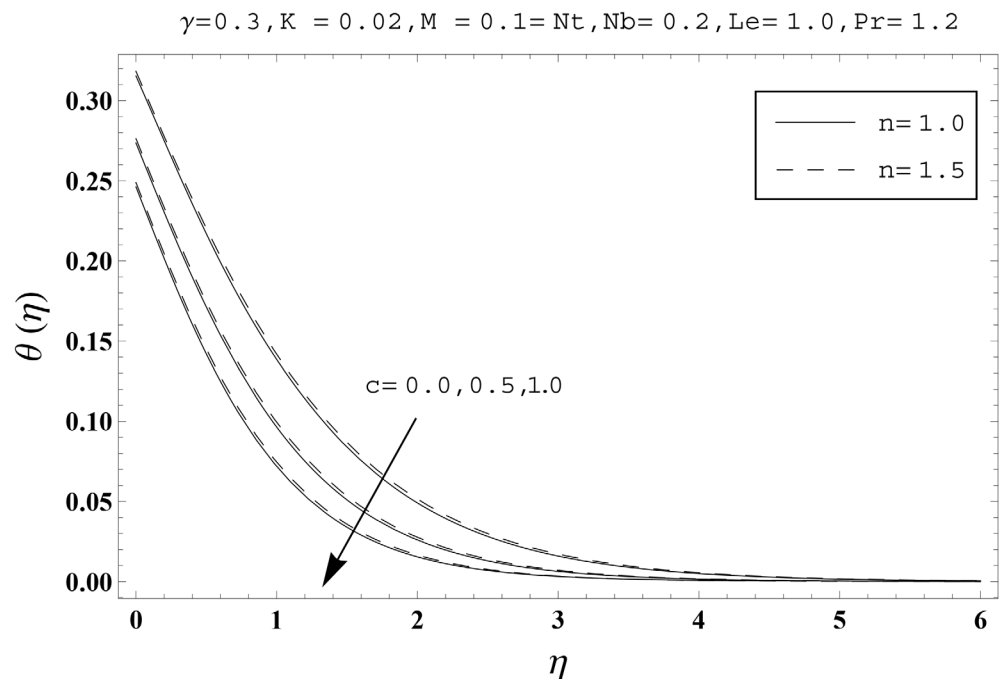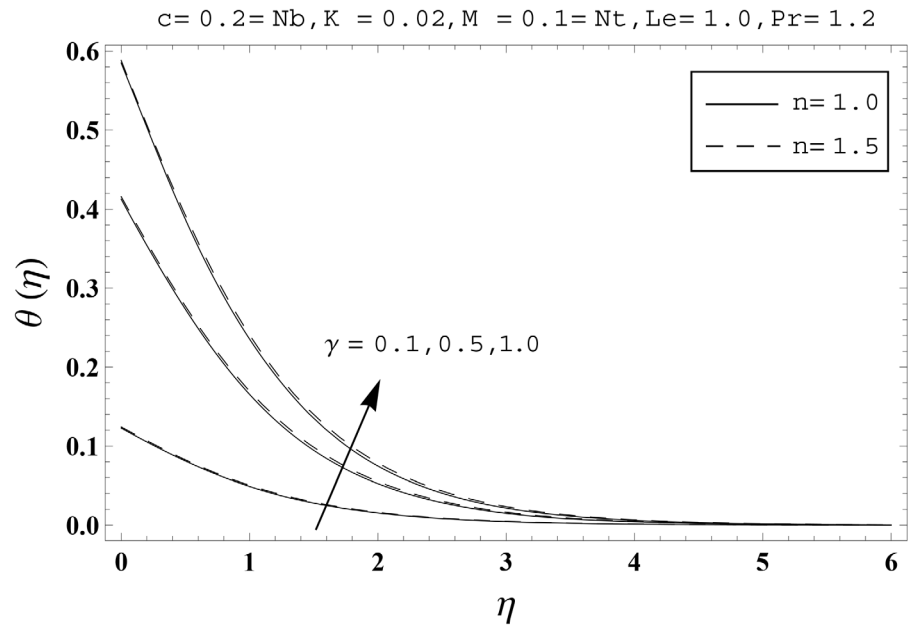
$\gamma = 0.3, K = 0.02, M = 0.1 = Nt, Nb = 0.2, Le = 1.0, Pr = 1.2$

Fig 5. Effects of *n* and *c* on *θ(η)*.

doi:10.1371/journal.pone.0145332.g005

Fig 6. Effects of *n* and *γ* on *θ(η)*.

concentration profiles corresponding to various values of couple stress parameter *K*. Larger values of couple stress parameter leads to stronger nanoparticles concentration distributions and more nanoparticles concentration boundary layer thicknesses. It is also shown that the nanoparticles concentration field is higher in nonlinear stretching surface case (*n* = 1.5) when compared with the linear stretching surface (*n* = 1.0). Fig 10 depicts that the nanoparticles

Fig 7. Effects of *n* and *Pr* on *θ(η)*.

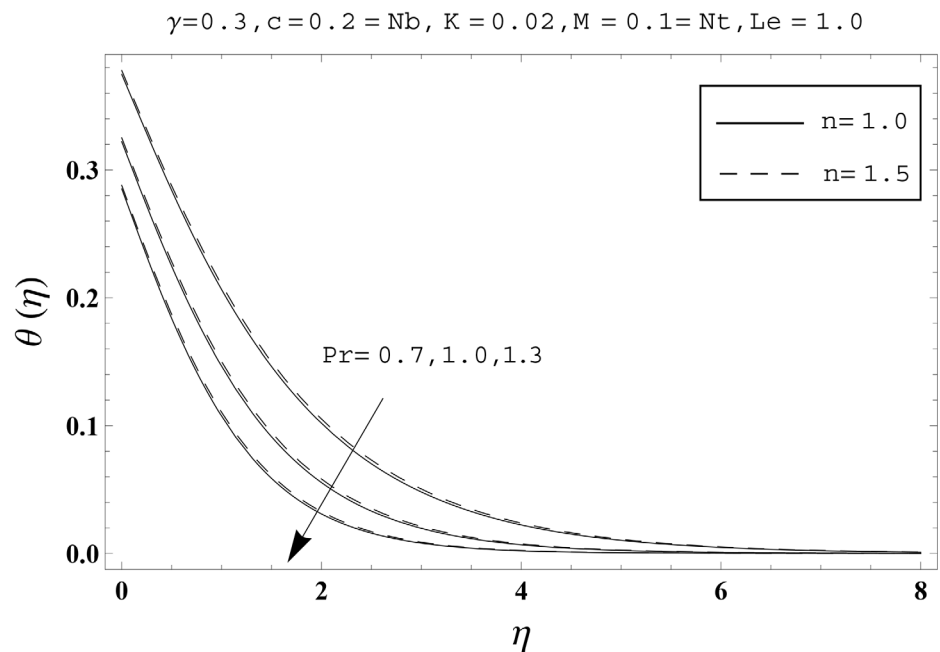$\gamma=0.3,c=0.2=Nb,K=0.02,M=0.1,Le=1.0,Pr=1.2$
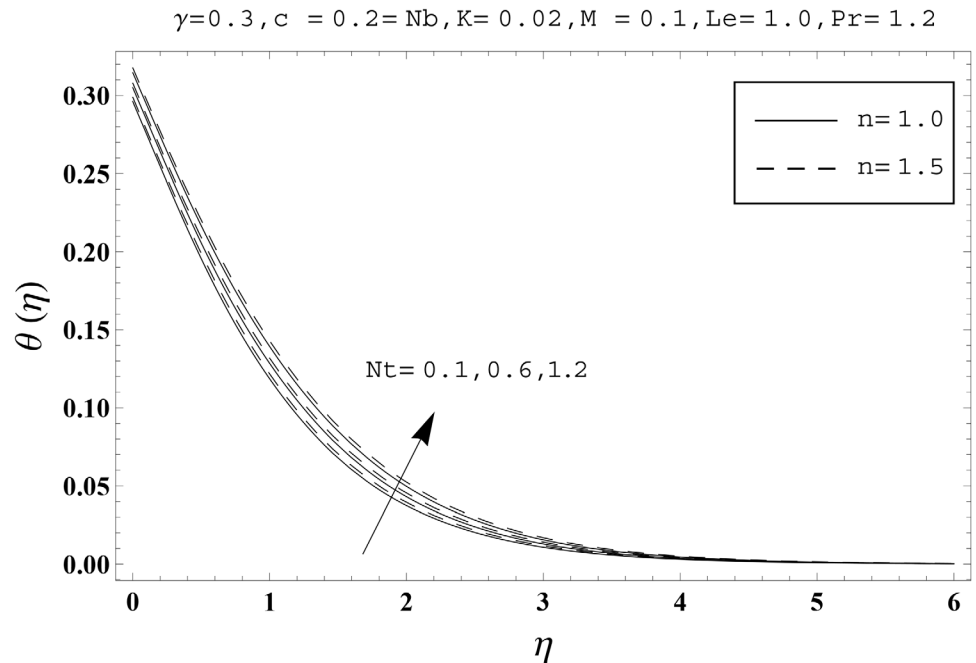
Fig 8. Effects of *n* and *Nt* on *θ(η)*.

doi:10.1371/journal.pone.0145332.g008

concentration profiles are enhanced when we increase the values of magnetic number M. Moreover the nanoparticles concentration profiles show similar behavior for both linear and nonlinear stretching surfaces. Fig 11 shows the nanoparticles concentration profiles corresponding to different values of the ratio parameter c. Here the nanoparticles concentration

$\gamma=0.3,c=0.2=Nb,M=0.1=Nt,Le=1.0,Pr=1.2$
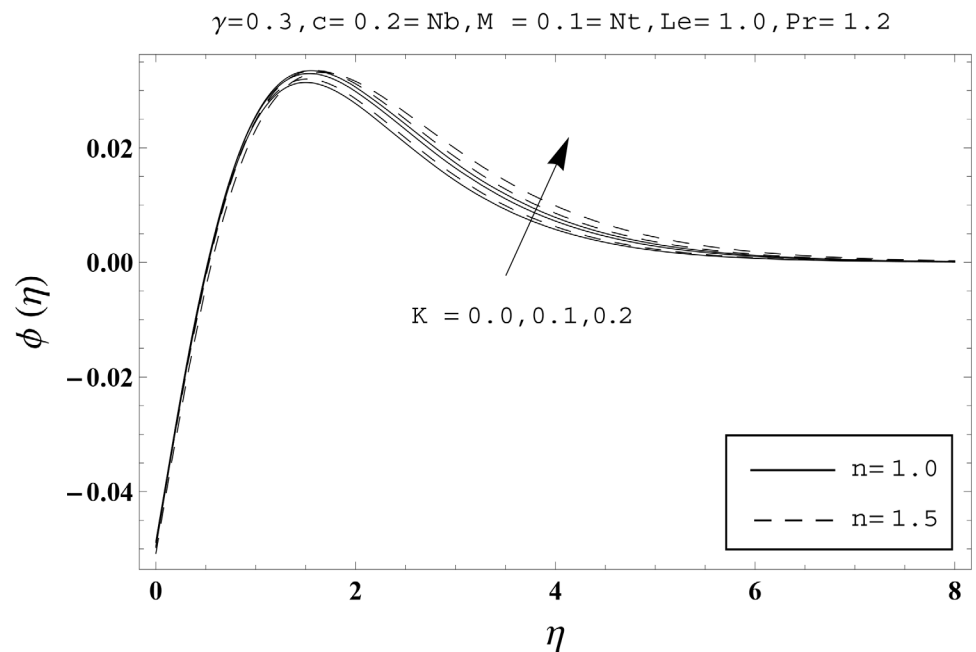
Fig 9. Effects of *n* and *K* on *ϕ(η)*.

doi:10.1371/journal.pone.0145332.g009

$\gamma=0.3, c=0.2= Nb, K = 0.02, Nt= 0.1, Le= 1.0, Pr= 1.2$
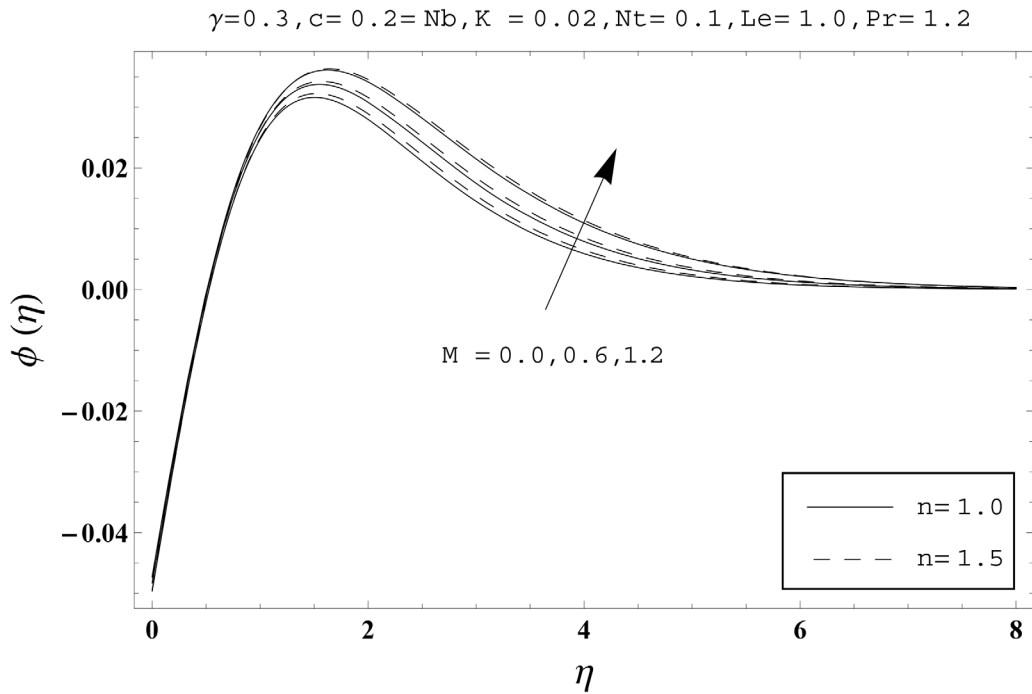
Fig 10. Effects of *n* and *M* on $\phi(\eta)$.

$\gamma=0.3, K = 0.02, M = 0.1= Nt, Nb= 0.2, Le= 1.0, Pr= 1.2$
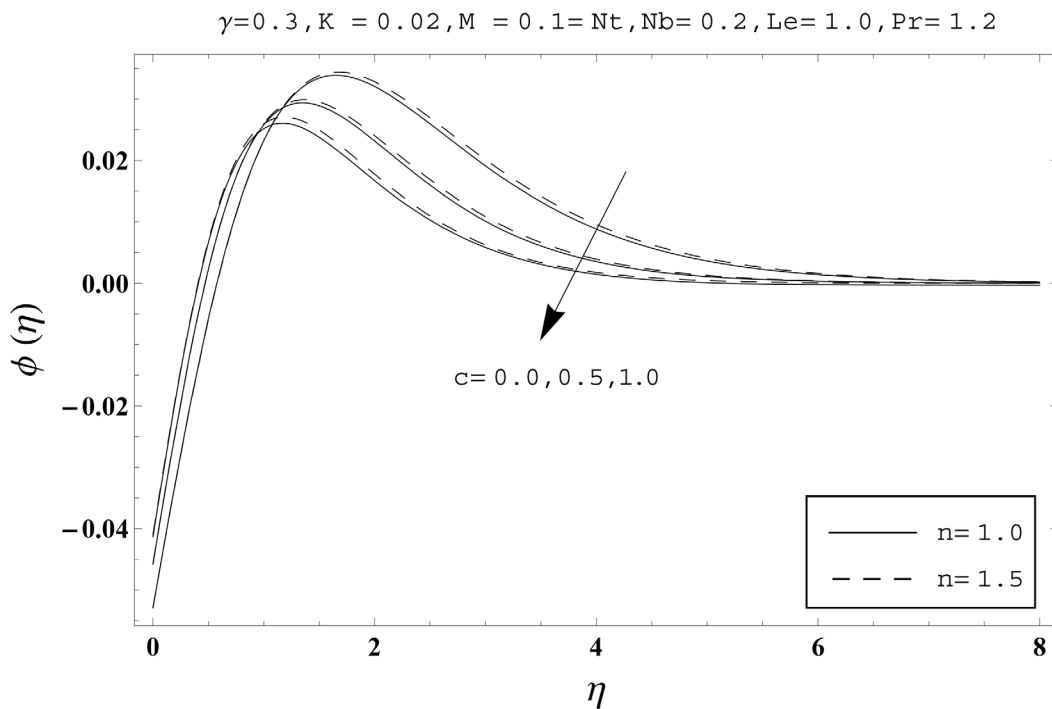
Fig 11. Effects of *n* and *c* on $\phi(\eta)$.
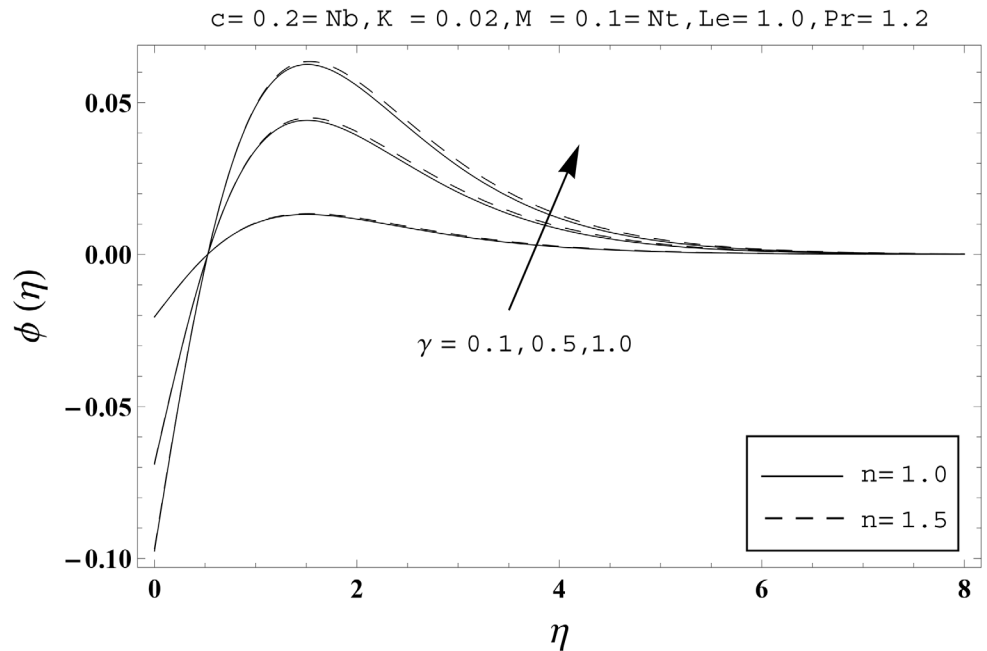
Fig 12. Effects of *n* and *γ* on $\phi(\eta)$.

profiles are lower for the larger values of ratio parameter. It is also noticed that the nanoparticles concentration profiles show decreasing behavior for both linear and nonlinear stretching surfaces. Effects of Biot number γ on the nanoparticles concentration distributions are presented in the Fig 12. Nanoparticles concentration profiles are higher for the larger values of Biot number. Moreover the nanoparticles concentration profiles show similar behavior for
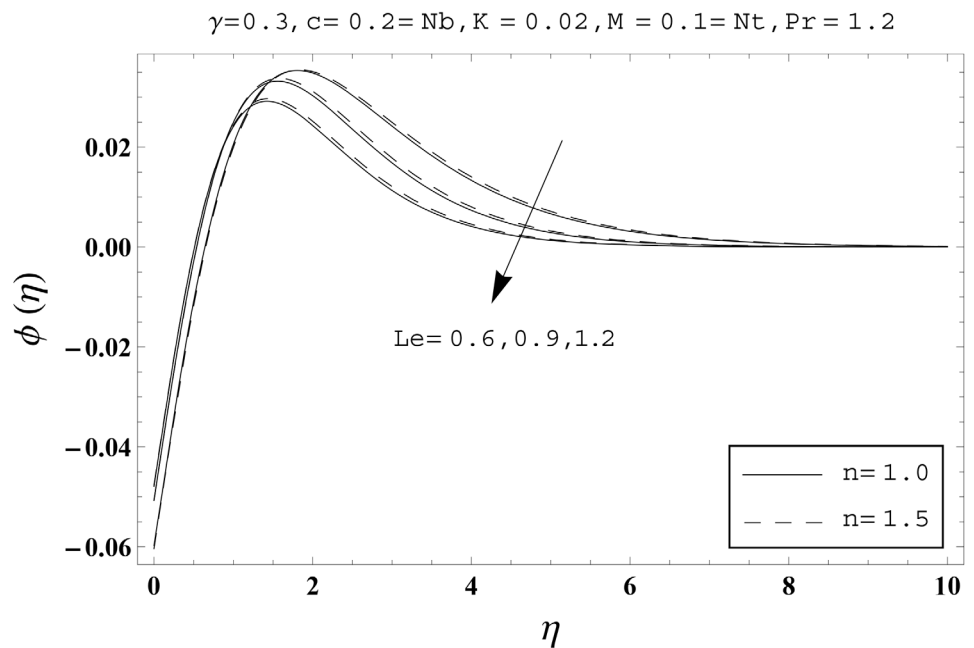
Fig 13. Effects of *n* and *Le* on $\phi(\eta)$.
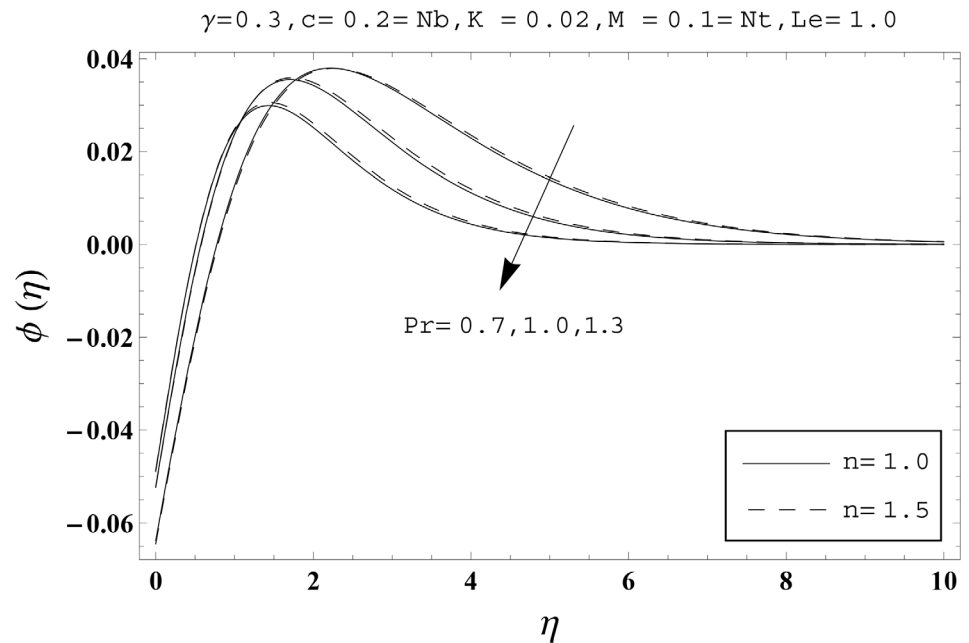
Fig 14. Effects of *n* and *Pr* on $\phi(\eta)$.

both linear and nonlinear stretching surfaces. Fig 13 presents that the nanoparticles concentration profiles are lower for the larger values of Lewis number *Le*. Lewis number has an inverse relationship with the Brownian diffusion coefficient. An enhancement in the Lewis number leads to a lower Brownian diffusion coefficient. Such lower Brownian diffusion coefficient

Fig 15. Effects of *n* and *Nb* on $\phi(\eta)$.

Fig 16. Effects of *n* and *Nt* on $\phi(\eta)$.

doi:10.1371/journal.pone.0145332.g016

causes weaker nanoparticles concentration profiles. It is also observed that the nanoparticles concentration distributions show decreasing behavior for both linear and nonlinear stretching surfaces. Effects of Prandtl number *Pr* on the nanoparticles concentration profiles are sketched in Fig 14. We observed that an enhancement in the Prandtl number produces weaker nanoparticles concentration profiles. Moreover the nanoparticles concentration profiles depict similar behavior for both linear and nonlinear stretching surfaces. Fig 15 shows that the larger values of Brownian motion parameter *Nb* creates lower nanoparticles concentration profiles. It is also seen that the nanoparticles concentration distributions are lower for both linear and nonlinear stretching surfaces. Effects of thermophoresis parameter *Nt* on the nanoparticles concentration profiles are presented in Fig 16. It is clearly observed that the nanoparticles concentration profiles are enhanced for the larger values of thermophoresis parameter. Moreover the 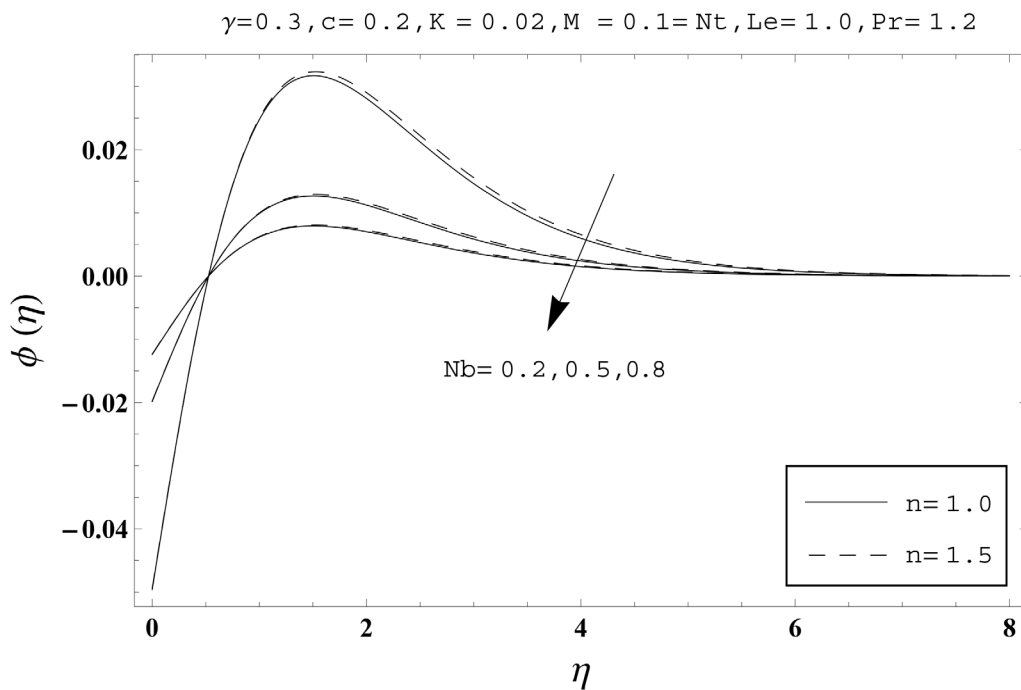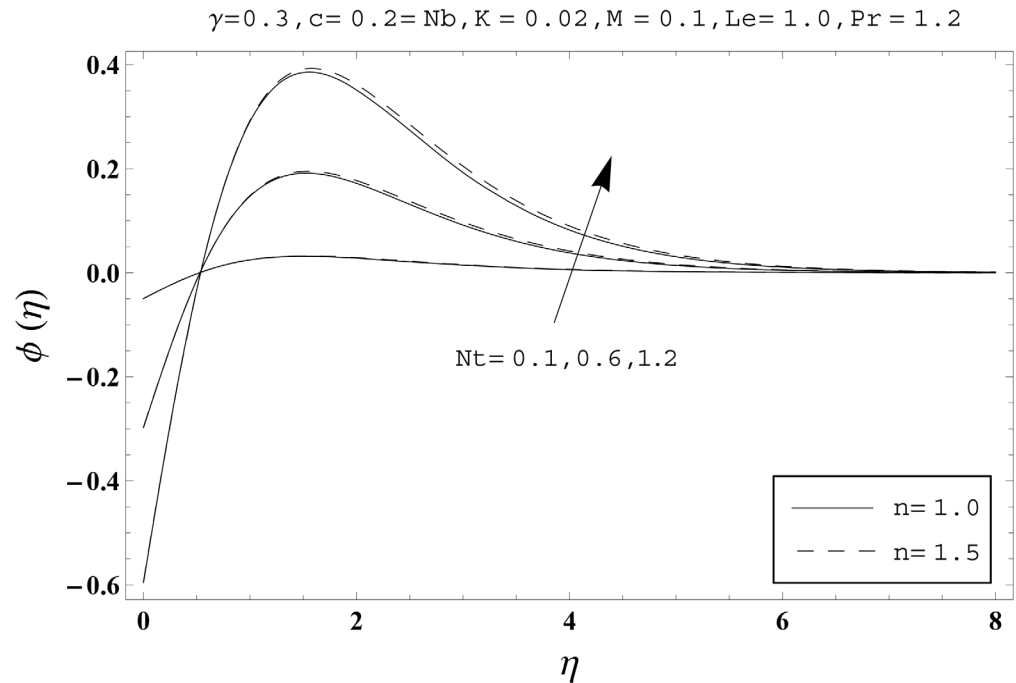nanoparticles concentration field is weaker for linear stretching surface (*n* = 1.0) when compared with the nonlinear stretching surface (*n* = 1.5). Table 2 depicts the values of skin-friction coefficients $-Re_x^{1/2}C_{fx}$ and $-Re_y^{1/2}C_{fy}$ for various values of power-law index *n*, couple stress parameter *K*, magnetic number *M* and ratio parameter *c*. Here the skin-friction coefficients are increasing functions of power-law index *n*. It is also seen that the skin-friction coefficients are enhanced for the larger values of magnetic number *M*. Values of local Nusselt number $Re_x^{-1/2}Nu_x$ for various values of *n*, *K*, *M*, *c*, *γ*, *Nt*, *Nb*, *Le* and *Pr* are computed in Table 3. We noticed that the larger values of couple stress parameter *K*, magnetic number *M* and thermophoresis parameter *Nt* correspond to a lower local Nusselt number while opposite behavior is observed for Biot number *γ*. Table 4 presents the values of temperature and nanoparticles concentration profiles for various values of *n*, *K*, *M*, *c*, *γ*, *Nt*, *Nb*, *Le* and *Pr* when *η* = 1.0. From this Table, it is clearly shown that the Biot number *γ* and Prandtl number *Pr* influences the temperature and nanoparticles concentration profiles the most.

Table 2. Values of skin-friction coefficients $-Re_x^{1/2}C_{fx}$ and $-Re_y^{1/2}C_{fy}$ for various values of n, K, M and c.

K	M	c	$-Re_x^{1/2}C_{fx}$		$-Re_y^{1/2}C_{fy}$	
			$n = 1.0$	$n = 1.5$	$n = 1.0$	$n = 1.5$
0.00	0.1	0.2	1.1000	1.3050	2.4597	2.9181
0.01			1.0932	1.2945	2.4446	2.8945
0.02			1.0863	1.2832	2.4290	2.8694
0.02	0.0	0.2	1.0819	1.2786	2.4192	2.8591
	0.2		1.0993	1.2970	2.4581	2.9001
	0.5		1.1860	1.3886	2.6520	3.1050
0.02	0.1	0.2	1.0863	1.2832	2.4290	2.8694
		0.3	1.1290	1.3332	2.0613	2.4341
		0.5	1.2095	1.4270	1.7105	2.0181

doi:10.1371/journal.pone.0145332.t002

Main findings

Three-dimensional flow of couple stress nanofluid over a nonlinear stretching surface with the convective surface boundary condition and non-uniform magnetic field is analyzed. The main findings of the present research are given below:

Table 3. Values of local Nusselt number $Re_x^{-1/2}Nu_x$ for various values of n, K, M, c, γ, Nt, Nb, Le and Pr.

K	M	c	γ	Nt	Nb	Le	Pr	$Re_x^{-1/2}Nu_x$	
								n = 1.0	n = 1.5
0.00	0.1	0.2	0.3	0.1	0.2	1.0	1.2	0.2114	0.2356
0.02								0.2112	0.2352
0.05								0.2108	0.2344
0.02	0.0	0.2	0.3	0.1	0.2	1.0	1.2	0.2113	0.2353
	0.5							0.2091	0.2329
	0.8							0.2060	0.2295
0.02	0.1	0.0	0.3	0.1	0.2	1.0	1.2	0.2054	0.2287
		0.3						0.2136	0.2379
		0.5						0.2180	0.2427
0.02	0.1	0.2	0.1	0.1	0.2	1.0	1.2	0.0877	0.0979
			0.7					0.3527	0.3917
			1.2					0.4458	0.4943
0.02	0.1	0.2	0.3	0.0	0.2	1.0	1.2	0.2115	0.2355
				0.5				0.2100	0.2338
				1.0				0.2084	0.2321
0.02	0.1	0.2	0.3	0.1	0.5	1.0	1.2	0.2112	0.2352
					1.0			0.2112	0.2352
					1.5			0.2112	0.2352
0.02	0.1	0.2	0.3	0.1	0.2	0.5	1.2	0.2113	0.2353
						1.0		0.2112	0.2352
						1.5		0.2111	0.2351
0.02	0.1	0.2	0.3	0.1	0.2	1.0	0.5	0.1687	0.1874
							1.0	0.2034	0.2263
							1.5	0.2200	0.2451

doi:10.1371/journal.pone.0145332.t003

Table 4. Values of temperature and nanoparticles concentration profiles for various values of *n*, *K*, *M*, *c*, *γ*, *Nt*, *Nb*, *Le* and *Pr* when *η* = 1.0.

K	M	c	γ	Nt	Nb	Le	Pr	Temperature		Concentration	
								n = 1.0	*n* = 1.5	*n* = 1.0	*n* = 1.5
0.1	0.1	0.2	0.3	0.1	0.2	1.0	1.2	0.12041	0.12292	0.01230	0.01133
0.3								0.12673	0.13022	0.00970	0.00823
0.5								0.13436	0.13885	0.00643	0.00447
0.02	0.1	0.2	0.3	0.1	0.2	1.0	1.2	0.11826	0.12038	0.01316	0.01238
	0.3							0.11989	0.12191	0.01257	0.01184
	0.5							0.12296	0.12479	0.01147	0.01084
0.02	0.1	0.1	0.3	0.1	0.2	1.0	1.2	0.12676	0.12867	0.01000	0.00928
		0.3						0.11035	0.11264	0.01605	0.01523
		0.5						0.09619	0.09871	0.02105	0.02022
0.02	0.1	0.2	0.1	0.1	0.2	1.0	1.2	0.04879	0.04969	0.00511	0.00478
			0.3					0.11826	0.12038	0.01316	0.01238
			0.5					0.16523	0.16810	0.01913	0.01807
0.02	0.1	0.2	0.3	0.1	0.2	1.0	1.2	0.11826	0.12038	0.01316	0.01238
				0.3				0.11927	0.12139	0.03941	0.03708
				0.5				0.12029	0.12241	0.06557	0.06167
0.02	0.1	0.2	0.3	0.1	0.1	1.0	1.2	0.11826	0.12038	0.02632	0.02476
					0.3			0.11826	0.12038	0.00877	0.00825
					0.5			0.11826	0.12038	0.00526	0.00495
0.02	0.1	0.2	0.3	0.1	0.2	0.1	1.2	0.11810	0.12022	-0.03558	-0.03568
						0.3		0.11813	0.12025	-0.02244	-0.02272
						0.5		0.11816	0.12028	-0.01056	-0.01101
0.02	0.1	0.2	0.3	0.1	0.2	1.0	0.1	0.25066	0.25086	-0.03989	-0.03997
							0.3	0.22398	0.22457	-0.02871	-0.02893
							0.5	0.19834	0.19930	-0.01815	-0.01851

doi:10.1371/journal.pone.0145332.t004

- An increase in the couple stress parameter *K* shows an enhancement in the temperature and nanoparticles concentration profiles.

- Temperature and nanoparticles concentration profiles are enhanced with an increase in the values of magnetic number *M*.

- Effects of Biot number *γ* on the temperature and nanoparticles concentration profiles are qualitatively similar.

- Temperature $θ(η)$ and thickness of the thermal boundary layer are lower for the larger values of Prandtl number *Pr*.

- Larger values of thermophoresis parameter *Nt* present similar behavior for temperature and nanoparticles concentration profiles.

- An enhancement in the Brownian motion parameter corresponds a weaker nanoparticles concentration profile.

- Coefficients of skin-friction are higher for the larger values of the magnetic number *M*.

- Rate of heat transfer at the wall is constant for Brownian motion parameter while it is lower for the thermophoresis parameter.

Author Contributions

Conceived and designed the experiments: TH AA TM BA. Performed the experiments: TH AA TM BA. Analyzed the data: TH AA TM BA. Contributed reagents/materials/analysis tools: TH AA TM BA. Wrote the paper: TH AA TM BA.

References

1. Vajravelu K. Viscous flow over a nonlinearly stretching sheet. Appl Math Comput. 2001; 124: 281–288.

2. Cortell R. Viscous flow and heat transfer over a nonlinearly stretching sheet. Appl Math Comput. 2007; 184: 864–873.

3. Cortell R. Effects of viscous dissipation and radiation on the thermal boundary layer over a nonlinearly stretching sheet. Phys Lett A. 2008; 372: 631–636.

4. Hayat T, Hussain Q, Javed T. The modified decomposition method and Padé approximants for the MHD flow over a non-linear stretching sheet. Nonlinear Anal-Real World Appl. 2009; 10: 966–973.

5. Rana P, Bhargava R. Flow and heat transfer of a nanofluid over a nonlinearly stretching sheet: A numerical study. Comm Nonlinear Sci Num Simulat. 2012; 17: 212–226.

6. Mukhopadhyay S. Analysis of boundary layer flow over a porous nonlinearly stretching sheet with partial slip at the boundary. Alexandria Eng J. 2013; 52: 563–569.

7. Mabood F, Khan WA, Ismail AIM. MHD boundary layer flow and heat transfer of nanofluids over a nonlinear stretching sheet: A numerical study. J Magn Magn Mater. 2015; 374: 569–576.

8. Mustafa M, Khan JA, Hayat T, Alsaedi A. Boundary layer flow of nanofluid over a nonlinearly stretching sheet with convective boundary condition. IEEE Trans Nanotech. 2015; 14: 159–168.

9. Choi SUS, Eastman JA. Enhancing thermal conductivity of fluids with nanoparticles. ASME International Mechanical Engineering Congress & Exposition, American Society of Mechanical Engineers, San Francisco 1995.

10. Boungiorno J. Convective transport in nanofluids. ASME J Heat Transfer. 2006; 128: 240–250.

11. Khan WA, Pop I. Boundary-layer flow of a nanofluid past a stretching sheet. Int J Heat Mass Transfer. 2010; 53: 2477–2483.

12. Pujari S, Rahatekar SS, Gilman JW, Koziol KK, Windle AH, Burghardt WR. Orientation dynamics in multiwalled carbon nanotube dispersions under shear flow. J Chem Phys. 2009; 130: 214903. doi: 10.1063/1.3139446 PMID: 19508094

13. Dong RY, Cao BY. Anomalous orientations of a rigid carbon nanotube in a sheared fluid. Sci Rep. 2014; 4: 6120. doi: 10.1038/srep06120 PMID: 25134626

14. Zhao Y, Zhao C, He J, Zhou Y, Yang C. Collective effects on thermophoresis of colloids: a microfluidic study within the framework of DLVO theory. Soft Matter. 2013; 9: 7726.

15. Dong RY, Zhou Y, Yang C, Cao BY. Translational thermophoresis and rotational movement of peanut-like colloids under temperature gradient. Microfluid Nanofluid. 2015; 19: 805–811.

16. Wang Z, Kriegs H, Buitenhuis J, Dhont JKG, Wiegand S. Thermophoresis of charged colloidal rods. Soft Matter. 2013; 9: 8697.

17. Turkyilmazoglu M. Exact analytical solutions for heat and mass transfer of MHD slip flow in nanofluids. Chem Eng Sci. 2012; 84: 182–187.

18. Ibrahim W, Makinde OD. The effect of double stratification on boundary-layer flow and heat transfer of nanofluid over a vertical plate. Comput Fluids. 2013; 86: 433–441.

19. Hsiao KL. Nanofluid flow with multimedia physical features for conjugate mixed convection and radiation. Comp Fluids. 2014; 104: 1–8.

20. Lin Y, Zheng L, Zhang X. Radiation effects on Marangoni convection flow and heat transfer in pseudo-plastic non-Newtonian nanofluids with variable thermal conductivity. Int J Heat Mass Transfer. 2014; 77: 708–716.

21. Zeeshan A, Baig M, Ellahi R, Hayat T. Flow of viscous nanofluid between the concentric cylinders. J Comp Theoretical Nanoscience. 2014; 11: 646–654.

22. Sheikholeslami M, Bandpy MG, Ellahi R, Hassan M, Soleimani S. Effects of MHD on Cu-water nanofluid flow and heat transfer by means of CVFEM. J Magn Magn Mater. 2014; 349: 188–200.

23. Zhang C, Zheng L, Zhang X, Chen G. MHD flow and radiation heat transfer of nanofluids in porous media with variable surface heat flux and chemical reaction. Appl Math Modell. 2015; 39: 165–181.

24. Sheikholeslami M, Ganji DD, Javed MY, Ellahi R. Effect of thermal radiation on magnetohydrodynamics nanofluid flow and heat transfer by means of two phase model. J Magn Magn Mater. 2015; 374: 36–43.

25. Gireesha BJ, Gorla RSR, Mahanthesh B. Effect of suspended nanoparticles on three-dimensional MHD flow, heat and mass transfer of radiating Eyring-Powell fluid over a stretching sheet. J Nanofluids. 2015; 4: 474–484.

26. Mustafa M, Khan JA, Hayat T, Alsaedi A. On Bödewadt flow and heat transfer of nanofluids over a stretching stationary disk. J Mol Liquids. 2015; 211: 119–125.

27. Hayat T, Imtiaz M, Alsaedi A. Impact of magnetohydrodynamics in bidirectional flow of nanofluid subject to second order slip velocity and homogeneous-heterogeneous reactions. J Magn Magn Mater. 2015; 395: 294–302.

28. Stokes VK. Couple stresses in fluids. Phys Fluids. 1966; 9: 1709–1715.

29. Srinivasacharya D, Kaladhar K. Mixed convection flow of couple stress fluid in a non-darcy porous medium with Soret and Dufour effects. J Appl Sci Eng. 2012; 15: 415–422.

30. Ramzan M, Farooq M, Alsaedi A, Hayat T. MHD three-dimensional flow of couple stress fluid with Newtonian heating. Eur Phys J Plus. 2013; 128: 49.

31. Hayat T, Mustafa M, Iqbal Z, Alsaedi A. Stagnation-point flow of couple stress fluid with melting heat transfer. Appl Math Mech -Eng Ed. 2013; 34: 167–176.

32. Turkyilmazoglu M. Exact solutions for two-dimensional laminar flow over a continuously stretching or shrinking sheet in an electrically conducting quiescent couple stress fluid. Int J Heat Mass Transfer. 2014; 72: 1–8.

33. Hayat T, Muhammad T, Alsaedi A, Alhuthali MS. Magnetohydrodynamic three-dimensional flow of viscoelastic nanofluid in the presence of nonlinear thermal radiation. J Magn Magn Mater. 2015; 385: 222–229.

34. Makinde OD, Aziz A. Boundary layer flow of a nanofluid past a stretching sheet with a convective boundary condition. Int J Thermal Sci. 2011; 50: 1326–1332.

35. Hayat T, Muhammad T, Shehzad SA, Chen GQ, Abbas IA. Interaction of magnetic field in flow of Maxwell nanofluid with convective effect. J Magn Magn Mater. 2015; 389: 48–55.

36. Kuznetsov AV, Nield DA. Natural convective boundary-layer flow of a nanofluid past a vertical plate: A revised model. Int J Thermal Sci. 2014; 77: 126–129.

37. Hayat T, Muhammad T, Shehzad SA, Alhuthali MS, Lu J. Impact of magnetic field in three-dimensional flow of an Oldroyd-B nanofluid. J Mol Liquids. 2015; 212: 272–282.

38. Liao SJ. Homotopy analysis method in nonlinear differential equations, Springer & Higher Education Press, Heidelberg, 2012.

39. Turkyilmazoglu M. Solution of the Thomas-Fermi equation with a convergent approach. Commun Nonlinear Sci Numer Simulat. 2012; 17: 4097–4103.

40. Sheikholeslami M, Hatami M, Ganji DD. Micropolar fluid flow and heat transfer in a permeable channel using analytic method. J Mol Liquids. 2014; 194: 30–36.

41. Abbasbandy S, Hayat T, Alsaedi A, Rashidi MM. Numerical and analytical solutions for Falkner-Skan flow of MHD Oldroyd-B fluid. Int J Numer Methods Heat Fluid Flow. 2014; 24: 390–401.

42. Sui J, Zheng L, Zhang X, Chen G. Mixed convection heat transfer in power law fluids over a moving conveyor along an inclined plate. Int J Heat Mass Transfer. 2015; 85: 1023–1033.

43. Ellahi R, Hassan M, Zeeshan A. Shape effects of nanosize particles in Cu-H_2O nanofluid on entropy generation. Int J Heat Mass Transfer. 2015; 81: 449–456.

44. Hayat T, Muhammad T, Shehzad SA, Alsaedi A. Temperature and concentration stratification effects in mixed convection flow of an Oldroyd-B fluid with thermal radiation and chemical reaction. Plos One. 2015; 10: e0127646. doi: 10.1371/journal.pone.0127646 PMID: 26102200

45. Hayat T, Muhammad T, Shehzad SA, Alsaedi A. A mathematical study for three-dimensional boundary layer flow of Jeffrey nanofluid. Z Naturforsch A. 2015; 70a: 225–233.